# Interpreting the Conductance Blockades of DNA Translocations through Solid-State Nanopores

Autumn T. Carlsen,[†] Osama K. Zahid,[†] Jan Ruzicka,[§] Ethan W. Taylor,[§] and Adam R. Hall[†,‡,*]

[†]Department of Biomedical Engineering and [‡]Comprehensive Cancer Center, Wake Forest University School of Medicine, Winston-Salem, North Carolina 27101, United States and [§]Joint School of Nanoscience and Nanoengineering, University of North Carolina Greensboro, Greensboro, North Carolina 27401, United States

ABSTRACT Solid-state nanopore electrical signatures can be convoluted and are thus challenging to interpret. In order to better understand the origin of these conductance changes, we investigate the translocation of DNA through small, thin pores over a range of voltage. We observe multiple, discrete populations of conductance blockades that vary with applied voltage. To describe our observations, we develop a simple model that is applicable to solid-state nanopores generally. These results represent an important step toward understanding the dynamics of the electrokinetic translocation process.
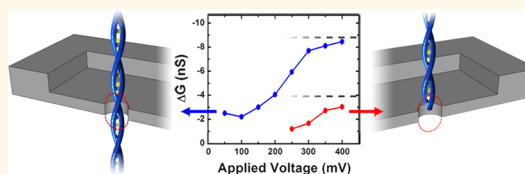
KEYWORDS: nanopore · DNA · translocation · conductance blockade · single molecule

Solid-state nanopores[1,2] are an emerging technology for rapid detection and characterization of biomolecules. In a typical measurement, an electric field is employed to drive individual molecules of RNA,[3] proteins,[4−7] and most often DNA[8,9] through a single aperture in a solid-state membrane (Figure 1a). The brief presence of the molecule within the opening is manifested as a shift in the measured electrical signal to one or more distinct levels of conductance, referred to as a blockade event. By virtue of their size, SS-nanopores are able to interrogate one or a few individual molecules at a time, and so they have proven to be an attractive possibility for a range of applications that require highly sensitive detection, perhaps most notably genetic sequencing.[10]

Although the operating principle of SS-nanopores is straightforward, the system is capable of exhibiting surprisingly complex behaviors that can make interpretation of the measured electrical signal challenging. One source of this complexity is thought to be interactions with the access regions[11]— the sensing volume immediately surrounding each opening of the aperture. Here, we seek to shed light on SS-nanopore measurements in general by investigating double-strand (ds) DNA conductance blockades systematically using a nanopore device with maximized contributions of the access regions to the sensing region. The access regions have long been an important consideration[12] in describing both cylindrical[13−19] and noncylindrical[20−23] nanopore systems. However, for SS-nanopores in extremely thin membranes[19] (<10 nm), these regions take on increased significance. We therefore initiate our study of conductance depth (ΔG) by investigating these unconventional devices.

RESULTS AND DISCUSSION

We begin by measuring 3 kbp dsDNA under high-ionic strength conditions with a single SS-nanopore (diameter 3.4 nm) fabricated in a 4.5 nm thick membrane. Previous work on devices with similar dimensions and under comparable solvent conditions demonstrated that dsDNA translocations produce deeper blockade events[19,24] compared to the typical 1−2 nS depth measured in conventional (thick) membranes.[3,8,9] Our measurements confirm this observation in general (Figure 1b). However, we arrive at a substantially more complex picture when we investigate the dependence of ΔG on applied voltage. Figure 1c shows all-points histograms for (concatenated) events over the range of 50−400 mV, with Gaussian fits (gray lines) indicating the locations of discrete conductance levels. From these data,
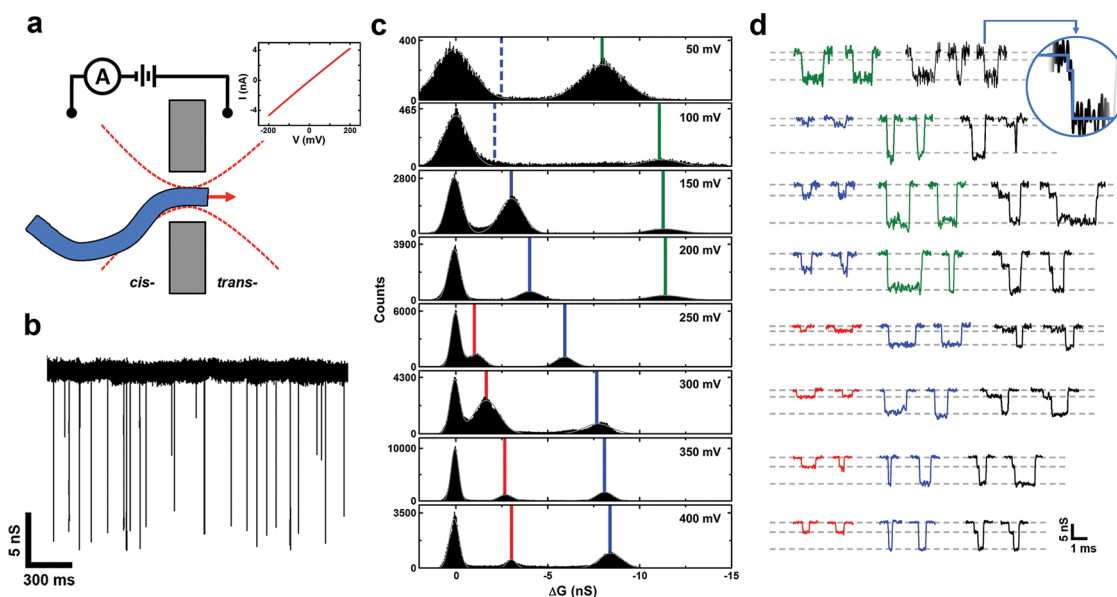
Figure 1. Conductance blockade measurements of dsDNA (a) Schematic representation of electrokinetic translocation from the *cis-* side of a SS-nanopore membrane to the *trans-* side. Inset shows the linear I−V characteristics of the device used here. **(b)** Typical conductance trace measured for 3 kbp dsDNA using a 4.5 nm thick, 3.4 nm diameter SS-nanopore. Voltage is 400 mV. **(c)** All-points histograms of (concatenated) conductance blockades from 50 to 400 mV (low-pass filtered at 10 kHz). In each panel, the left-most peak corresponds to the baseline (open-pore) conductance. Vertical lines indicate the center of the Gaussian fit (gray line) and indicate the evolution of individual conductance populations designated by color. **(d)** Example event traces for each applied voltage in (c). Dashed lines in background designate the discrete populations from the histograms to the left. Trace colors indicate the conductance level population of the event from (c), except the black traces, which correspond to events containing more than one level. The inset offers a magnified view of the indicated combination event, highlighting the brief initial shallow level. Note that this level is not resolvable in the 50 or 100 mV histograms (see text), but its position is indicated by dashed blue lines. All traces are low-pass filtered at 20 kHz. The scale bar applies to all traces.

we make two observations. First, we generally do not observe that the conductance blockade level resides exclusively at a single level, as may be expected for head-to-tail translocation of dsDNA through an aperture that is too narrow to allow the passage of folded molecules. Instead, we observe two well-separated levels of conductance under most conditions. These levels are not mutually exclusive, however, as we note that combination events occur regularly (black traces in Figure 1d). Second, the ΔG levels themselves shift significantly as the applied voltage is increased. Examining the evolution of blockade levels as a function of voltage (Figure 1c) reveals that three distinct populations are detected, each of which appears to increase in depth as applied voltage is increased.

We address the first of these observations by hypothesizing that the plurality of conductance blockade levels is the result of nontranslocative interactions with our device. This hypothesis is supported by the observed voltage dependence of mean event dwell time measurements (see the Supporting Information, Figure S-2). Recent work from several groups has suggested that unexpected levels of ΔG measured under certain experimental conditions are a result of dsDNA entering the access region, either stochastically[25,26] or as a precursor to translocation.[27−29] In order to describe the conductance blockades that may be expected from this type of interaction, we utilize a
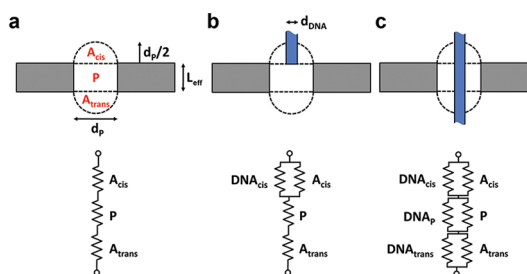

Figure 2. Components of the model. (a) Schematic of the three series conductances that form the sensing region of a SS-nanopore (gray): the pore (*P*) and the two hemispherical access regions (A_{cis} and A_{trans}, respectively). Models of DNA interaction with **(b)** one access region only (*case 1* from the text) and **(c)** all three regions (*case 2* from the text). Below each diagram is an equivalent circuit (conductances shown as resistors) representing the contributions of the three sensing regions listed above as well as that of the presence of the DNA in A_{cis} (designated DNA_{cis}), *P* (designated DNA_P), and A_{trans} (designated DNA_{trans}). Not shown are contributions of counterions surrounding the DNA, which act as an additional parallel conductance in each of the three regions.

model in which the SS-nanopore sensing region is composed of three relevant sections, the interior of the nanopore itself and the two access regions on either side (Figure 2a), following past work.[14,17] The conductance of each access region can be expressed simply[11] as

$$G_{0acc} = 2\sigma d_p \qquad (1)$$

where d_p is nanopore diameter and σ is the conductivity of the solution, defined as $(\mu_{cation} + \mu_{anion})ne$. Here, n is the number density (proportional to concentration) of the ionic species, e is the elementary charge, and μ_{cation} and μ_{anion} are electrophoretic mobilities of the cation and anion, respectively. The conductance of the pore, meanwhile, is

$$G_{0_{pore}} = \frac{\pi d_p^2}{4L_{eff}}\left(\sigma + \frac{4S\mu_{cation}}{d_p}\right) \quad (2)$$

where L_{eff} is the effective thickness of the membrane and S is the surface charge density[30] of the nanopore walls (taken[31] as 0.06 C/m²). We use the convention of Wanunu et al.[19] who established experimentally that $L_{eff} = L/3$, where L is the initial membrane thickness, to account for the noncylindrical shape of the nanopore. Because these conductances are in series, the total open-pore conductance of the system can thus be written as

$$G_{0_{TOTAL}} = \left(\frac{1}{G_{0_{pore}}} + \frac{2}{G_{0_{acc}}}\right)^{-1} \quad (3)$$

Generally, the presence of dsDNA in any of the sensing regions described above will act as a negative parallel conductance, displacing volume that would otherwise contribute to the total measured conductance. In order to quantify the effect, we consider two basic scenarios in relation to our data, taking into account that conductance can be expressed generally as $\sigma(A/l)$, where A is area and l is length.

In *case 1* (Figure 2b), the dsDNA is positioned coaxially with the mouth of the pore such that it interacts only with a single access region. Although the dsDNA could adopt a range of orientations with respect to this region, the geometry considered here can be considered a maximimum as it occupies the most space within the access region. In this scenario, the effect on the conductance of the occluded access region is

$$G_{acc_{DNA}} = G_{0_{acc}} - G_{DNA_{acc}} = G_{0_{acc}} - \sigma\frac{\pi d_{DNA}^2}{2d_p} \quad (4)$$

where d_{DNA} is the diameter of dsDNA, taken to be 2.2 nm. Note that in this case, the pertinent length of DNA, l, is the length of the access region ($d_p/2$). All other regions will be unchanged. As a result, the total change in conductance can be expressed as

$$\Delta G_{case1} = \left(\frac{1}{G_{0_{pore}}} + \frac{1}{G_{0_{acc}}} + \frac{1}{G_{acc_{DNA}}}\right)^{-1} - G_{0_{TOTAL}} \quad (5)$$

In *case 2*, the dsDNA is present in all three regions of the system (Figure 2c). As such, both access regions are affected as described in eq 4, and additionally, the conductance of the nanopore region is altered, as described by

$$G_{pore_{DNA}} = G_{0_{pore}} - G_{DNA_{pore}} = G_{0_{pore}} - \sigma\frac{\pi d_{DNA}^2}{4L_{eff}} \quad (6)$$
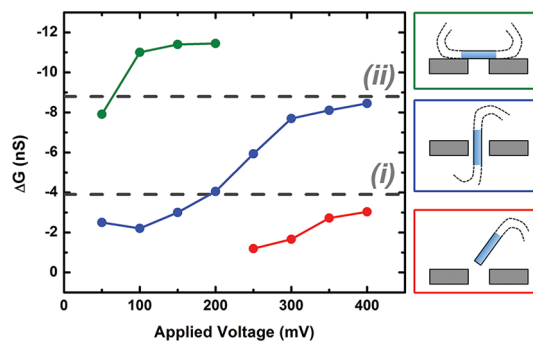

Figure 3. Analysis of dsDNA conductance blockades (a) Mean conductance change *vs* applied voltage. The dashed lines (*i*) and (*ii*) represent the calculated ΔG from eqs 5 (*case 1*, corresponding to nontranslocative events) and 7 (*case 2*, corresponding to translocation), respectively. Each point is the center of a Gaussian fit to the relevant histogram of all recorded events in Figure 1c, except the blue points at 50 and 100 mV, which are Gaussian fit centers from an all-points histogram of events containing the lower (2−2.5 nS) level. Schematics to the right illustrate the DNA configuration we propose for each population. Colors match those in in Figure 1c.

In total, this results in an expected conductance change for *case 2* of

$$\Delta G_{case2} = \left(\frac{1}{G_{pore_{DNA}}} + \frac{2}{G_{acc_{DNA}}}\right)^{-1} - G_{0_{TOTAL}} \quad (7)$$

The intermediate case, in which the dsDNA resides only in the *cis*-side access region and the nanopore is transitional since passage to the *trans*-side access region (*i.e., case 2*) is almost immediate from this state. As such, we consider it unlikely to be observed.

Equations 5 and 7 can be applied to our data by incorporating the device dimensions (d_p = 3.4 nm, $L_{eff} = L/3$ = 1.5 nm) and solvent conditions used in the experiment. Doing so yields for *case 1* a ΔG of −3.9 nS and for *case 2* a ΔG of −8.8 nS. In Figure 3a, we plot the mean conductance blockade levels over all investigated voltages, showing that the measured ΔG of each population increases and then saturates. Strikingly, the conductance levels predicted by our simple model (dashed lines in Figure 3a) match very closely the saturation conductance observed for two of the event populations from the experimental data. This indicates that at high voltages ($\geq$250 mV) for our device, the large ΔG level corresponds to true molecular translocations while the low ΔG level indicates nontranslocative interactions with the access region. We note that this model can be used similarly to predict the apparent saturation conductance change for results on voltage dependence of ΔG published elsewhere[3,32,33] (see the Supporting Information, Figure S-3).

Our model accounts for two populations within our data, but what is the origin of the third? One possibility may be that this level of conductance blockade is caused by a molecule approaching the SS-nanopore such that it lays perpendicular to the axis of the

aperture.[25,27−29,34] In this case, the stiffness of the molecule would prevent it from passing through the pore in a folded state, but the ion conductance would be blocked by its presence. The simplest approximation of this arrangement is that the area occupied by the dsDNA above the opening reduces the effective diameter of the SS-nanopore during its residence. If we assume a circular pore in the blocked case, this reduced effective pore diameter, d^*_p, can be expressed geometrically (see the Supporting Information, Figure S-4) by the equation

$$d^*_p = \sqrt{\frac{2}{\pi}\left(d_p^2 \cos^{-1}\left(\frac{d_{DNA}}{d_p}\right) - d_{DNA}(d_p^2 - d_{DNA}^2)^{1/2}\right)}$$

(8)

This assumes that the dsDNA sits directly across the center of the SS-nanopore. We arrive at an expected ΔG for the perpendicular case by simply calculating the difference between the conductance of the unoccluded pore with diameter d_p and the conductance of a pore with diameter d^*_p using eq 3. For our experimental conditions, ΔG for lateral blocking of the pore is found to be −15 nS. Since this can be considered a maximum (i.e., the dsDNA may not interact symmetrically across the center of the pore), the value is in qualitative agreement with the maximum conductance blockade recorded for the uncategorized population in Figure 3a of about −12 nS. We therefore conclude that this population is likely to correspond to lateral, nontranslocative interactions of the dsDNA with the SS-nanopore.

Identification of each conductance population presents further insight into the translocation process. As seen in Figure 1d, discrete conductance levels occur not only independently in single-level events, but also in combination to form two-level events. Interestingly, we observe that the shallow conductance level precedes the deep level for nearly all two-level events recorded across the entire investigated voltage range (543 out of 553, or 98.2%). At high voltages (≥250 mV), this ordering suggests an initial time period during which the end of the dsDNA is positioned in the access region of the SS-nanopore prior to threading through the aperture. The initial lag may correspond to repositioning or unfolding of the ensuing length of the molecule[35,36] (see the Supporting Information, Figure S-5). At low voltages (≤200 mV), the shallow-to-deep progression of conductance levels suggests instead that a portion of the dsDNA is threaded through the nanopore prior to lateral interactions between the remainder of the molecule and the aperture. We attribute these lateral interactions to the diminished capacity of the low-voltage electric field gradient to overcome the entropy of the dsDNA near the SS-nanopore.[26] Thus, the end of a threading molecule drags the entropic coil to the aperture en bloc, where it creates a deeper blockade as the translocation process continues. As voltage is reduced further, the likelihood of a molecular end being made available by the weaker electric field gradient is also reduced. Thus, at very low voltage, we would expect the shallow event level corresponding to translocation to be rare. This is indeed the case; the translocation ΔG level is uncommon at both 50 and 100 mV, and in conjunction with the low signal-to-noise ratio at these voltages, it is not distinguishable in an all-points histogram (see Figure 1c). However, the lower level can be resolved within individual blockade events (Figure 1d, top panel). Besides serving as additional support for our interpretation, this observation also offers an explanation as to why the ΔG level corresponding to lateral interactions with the SS-nanopore is seen exclusively at low voltage: at voltages greater than 200 mV, the large electric field gradient and increased viscous drag act to uncoil the dsDNA in solution before it reaches the pore.[37] Note that the deep ΔG level does not necessarily preclude molecular translocation at low voltage. Indeed, the blockade caused by the entropic coil may be able to simply mask the signal of the simultaneous threading of dsDNA through the pore.

While our model explains a great deal of what we observe in experiment, one central question remains: why do the conductance blockade levels increase and then saturate with applied voltage? Recently, several groups have reported similar behavior in conventional SS-nanopores,[3,32,33] but so far, an explanation has not been agreed upon. We suggest that the origin of this effect may be polarization of the dsDNA counterion cloud. The presence of positive charges surrounding the negatively charged dsDNA backbone is known to counteract the conductance blockade by introducing additional carriers to the sensing region.[30] However, theoretical work by Mendel[38] and later refinement by Manning[39] and others[40,41] has predicted that the local density of these counterions can be perturbed under extreme electric fields. Counterion polarization has since been observed through simulation[42−44] and experiment[45−47] and has recently been suggested as a potential factor in SS-nanopore measurements as well.[48,49] Perturbation of the counterion cloud could remove charge carriers locally from the sensing region of a nanopore, resulting in a voltage-dependent conductance blockade. Note that this local perturbation does not contradict overall electroneutrality as has been observed in molecular dynamics simulations.[50,51] Rather, the reduction in counterion density local to the sensing region of the nanopore would be accompanied by an equivalent buildup of charge outside the sensing region, as shown schematically in Figure 4 and in more detail in Figure S-6 (Supporting Information). In addition, because polarization will saturate at very high
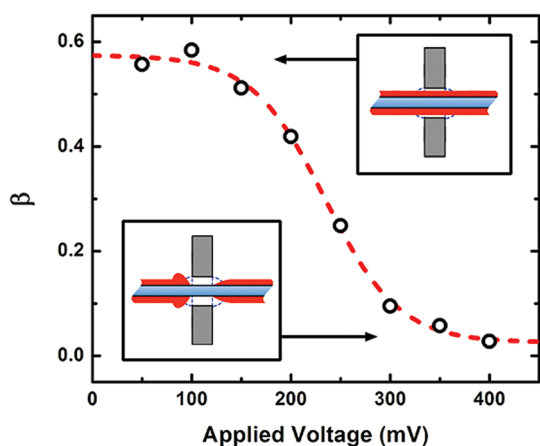
Figure 4. Counterion residence on translocating dsDNA The fraction of Na counterion charge (relative to the charge density of the dsDNA backbone) β vs applied voltage. Dashed line is a Boltzmann sigmoid fit to the data. Insets show schematic interpretation of the low-voltage case (top), where counterions remain bound to the DNA, and the high-voltage case (bottom), where counterions are displaced locally during translocation. In both images, DNA motion is toward the right. A more detailed schematic treatment is provided in the Supporting Information (Figure S-6).

electric field strength,[39] the voltage-dependence would likewise saturate at high voltage. These two key expectations match our experimental results well.

Counterion screening and polarization can be included in our model through a simple adjustment to eqs 4 and 6

$$G_{acc_{DNA}} = G_{0_{acc}} - G_{DNA_{acc}} + G_{counter_{acc}}$$

$$= G_{0_{acc}} - G_{DNA_{acc}} + \beta \frac{2q l \mu_{cation}}{d_p} \qquad (9)$$

$$G_{pore_{DNA}} = G_{0pore} - G_{DNA_{pore}} + G_{counter_{pore}}$$

$$= G_{0pore} - G_{DNA_{pore}} + \beta \frac{q \mu_{cation}}{L_{eff}} \qquad (10)$$

where q is the charge per unit length of dsDNA. We introduce β to denote the fractional effect of the new term relative to the zero-field counterion density, indicating polarization-induced depletion in the sensing region of the nanopore. When $\beta = 1$, the charge of the counterion cloud is exactly equivalent to that of the dsDNA itself. When $\beta = 0$, no counterions are present on the dsDNA in the sensing region and volumetric blocking is the only contribution to the conductance change (an alternative conceptualization is that β is indicative of a voltage-dependent shift in counterion mobility μ_{cation} rather than total counterion residence in the sensing region, though it is unclear by what mechanism this effect might saturate). So far, our model has assumed intrinsically that $\beta = 0$, resulting in good agreement with measurements at high voltage where polarization fully depletes of counterions in the pore. The transition toward this state can be

analyzed further by using eqs 9 and 10 to determine the β necessary to account for the measured voltage dependence of the ΔG. Such an analysis (Figure 4) suggests that the fractional residence of counterions around the dsDNA in the sensing region of the SS-nanopore decreases with voltage in a sigmoidal fashion. This data can be extrapolated to yield the zero-field value, which is $\beta = 0.57$ for our system. This value may be indicative of the fraction of counterions relative to the total dsDNA charge in the sensing region that are bound tightly to the molecule (resident in the major and minor grooves,[52] for example) under our solvent conditions (see the Supporting Information, Figure S-7). We note that β would represent an axial average along the length of the sensing region due to the axial inhomogeneity of the electric field in the nanopore. This approach may offer a general route toward probing the screening of polymers and biopolymers by arbitrary ionic species at various concentrations.

CONCLUSIONS

In conclusion, we have investigated dsDNA conductance blockades with a small diameter (3.4 nm) SS-nanopore formed in a thin (4.5 nm) membrane. We measured across a range of applied voltage and found that (i) three discrete levels of conductance change can be observed and (ii) the ΔG associated with these levels becomes larger as the voltage is increased. We presented a simple model that takes into account the access regions of the SS-nanopore device and considers both the volume of the dsDNA and its accompanying countercharge layer as parallel conductances to that of the nanopore itself. We found that this model describes accurately the conductance blockade levels measured experimentally and additionally provides a possible explanation for the observed voltage dependence of ΔG. We proposed that the intensifying electric field that accompanies increasing voltage progressively removes the counterions surrounding the dsDNA in solution until eventually ion exclusion is the only contribution to the measured conductance change. Our results are widely applicable to a variety of experimental conditions and represent an important step toward understanding the meaning of SS-nanopore electrical signals in general. Indeed, our model can also be used to describe the observations of several previous studies using a variety of experimental conditions (see the Supporting Information, Figures S-3 and S-8). We note that while qualitative agreement is observed in all ionic conditions, quantitative agreement between our model and experimental work is currently limited to high-ionic strength solutions (see the Supporting Information, Figure S-9). Extension to the low-ionic strength regime should be possible with refinement.

In conventional systems, the multiple conductance blockade populations described here will be subtle.

For example, under typical solvent conditions (1 M KCl) for a SS-nanopore device with diameter and membrane thickness values of 20 nm each, the ΔG predicted for nontranslocative interactions with the access region would be expected to have a maximum value of only -0.7 nS in the high-voltage ($\beta = 0$) limit. Event duration would also be expected to be very brief under these high voltage conditions, and so as a result, reduction of the noise floor to a point where such

events would be measurable is likely to filter them out entirely. This may explain why the effect has not been described previously. As device diameter or membrane thickness is reduced, however, the influence of the access regions will become more conspicuous. For this reason, the current trend of the field toward SS-nanopore devices with small diameters[53] or low dimensionality[54−58] will be especially aided by consideration of our findings in order to assess results accurately.

MATERIALS AND METHODS

Solid-State Nanopore Fabrication. Silicon chips, each supporting a window of silicon nitride (24.5 nm thick as measured by ellipsometry), were purchased commercially (Norcada, Inc., Alberta, Canada). Thin SS-nanopores were produced with helium ion microscope fabrication by first reducing the local membrane thickness controllably[59] and then milling material from the center of the thinned region using a timed exposure.[33] The region around the pore was processed to have a final thickness of 4.5 ± 0.6 nm, as judged by two separate calibration strategies.[59,60] The precise diameter of the SS-nanopore was determined by applying the measured current−voltage characteristics of the device to eq 3 from the text and solving for d_p. The device exhibited a linear I−V curve and had a low-noise baseline conductance of 27.5 nS that varied less than 5% during the duration of the measurements.

DNA Translocation Measurements. Solvent conditions used for the presented measurements were 900 mM NaCl, 10 mM tris, 1 mM EDTA. dsDNA (3 kbp) was introduced to the *cis* side of the SS-nanopore at a concentration of ∼10 ng/μL. Conductance blockade events were recorded at a bandwidth of 200 kHz and with a 100 kHz four-pole Bessel filter applied. An additional low-pass filter of $10-20$ kHz was applied during analysis (as indicated in figure captions), which was performed using custom LabView software. Histograms from Figure 1c (and scatter plots in the Supporting Information, Figure S-1) are composed of $n = $ 96 (50 mV), 146 (100 mV), 426 (150 mV), 298 (200 mV), 437 (250 mV), 814 (300 mV), 542 (350 mV), and 616 (400 mV). Only events with durations between 100 μs and 2 ms were considered in our analysis.

Conflict of Interest: The authors declare no competing financial interest.

Supporting Information Available: Scatter plots of all measured blockade events, dwell time analysis, additional figures and text describing the application of the presented model to published results, and derivation of lateral nanopore blocking expression (eq 8). This material is available free of charge *via* the Internet at http://pubs.acs.org.

REFERENCES AND NOTES

1. Dekker, C. Solid-State Nanopores. *Nat. Nanotechnol.* **2007**, *2*, 209–215.
2. Wanunu, M. Nanopores: A Journey Towards DNA Sequencing. *Phys. Life Rev.* **2012**, *9*, 125–158.
3. Skinner, G. M.; van den Hout, M.; Broekmans, O.; Dekker, C.; Dekker, N. H. Distinguishing Single- and Double-Stranded Nucleic Acid Molecules Using Solid-State Nanopores. *Nano Lett.* **2009**, *9*, 2953–2960.
4. Firnkes, M.; Pedone, D.; Knezevic, J.; Doeblinger, M.; Rant, U. Electrically Facilitated Translocations of Proteins Through Silicon Nitride Nanopores: Conjoint and Competitive Action of Diffusion, Electrophoresis, and Electroosmosis. *Nano Lett.* **2010**, *10*, 2162–2167.
5. Fologea, D.; Ledden, B.; McNabb, D. S.; Li, J. Electrical Characterization of Protein Molecules By a Solid-State Nanopore. *Appl. Phys. Lett.* **2007**, 91.
6. Han, A. P.; Schurmann, G.; Mondin, G.; Bitterli, R. A.; Hegelbach, N. G.; de Rooij, N. F.; Staufer, U. Sensing Protein Molecules Using Nanofabricated Pores. *Appl. Phys. Lett.* **2006**, 88.
7. Plesa, C.; Kowalczyk, S. W.; Zinsmeester, R.; Grosberg, A. Y.; Rabin, Y.; Dekker, C. Fast Translocation of Proteins Through Solid-State Nanopores. *Nano Lett.* **2013**, *13*, 658–663.
8. Li, J. L.; Gershow, M.; Stein, D.; Brandin, E.; Golovchenko, J. A. DNA Molecules and Configurations in a Solid-State Nanopore Microscope. *Nat. Mater.* **2003**, *2*, 611–615.
9. Storm, A. J.; Chen, J. H.; Zandbergen, H. W.; Dekker, C. Translocation of Double-Strand DNA through a Silicon Oxide Nanopore. *Phys. Rev. E* **2005**, 71.
10. Branton, D.; Deamer, D. W.; Marziali, A.; Bayley, H.; Benner, S. A.; Butler, T.; Di Ventra, M.; Garaj, S.; Hibbs, A.; Huang, X.; et al. The Potential and Challenges of Nanopore Sequencing. *Nat. Biotechnol.* **2008**, *26*, 1146–1153.
11. Hall, J. E. Access Resistance of a Small Circular Pore. *J. Gen. Physiol.* **1975**, *66*, 531–532.
12. Willmott, G. R.; Smith, B. G. Comment on 'Modeling the Conductance and DNA Blockade of Solid-State Nanopores'. *Nanotechnology* **2012**, *23*, 088001.
13. Bacri, L.; Oukhaled, A. G.; Schiedt, B.; Patriarche, G.; Bourhis, E.; Gierak, J.; Pelta, J.; Auvray, L. Dynamics of Colloids in Single Solid-State Nanopores. *J. Phys. Chem. B* **2011**, *115*, 2890–2898.
14. Hyun, C.; Rollings, R.; Li, J. Probing Access Resistance of Solid-State Nanopores With a Scanning-Probe Microscope Tip. *Small* **2012**, *8*, 385–392.
15. Kowalczyk, S. W.; Grosberg, A. Y.; Rabin, Y.; Dekker, C. Modeling the Conductance and DNA Blockade of Solid-State Nanopores. *Nanotechnology* **2011**, *22*, 315101.
16. Sun, L.; Crooks, R. M. Single Carbon Nanotube Membranes: A Well-Defined Model for Studying Mass Transport Through Nanoporous Materials. *J. Am. Chem. Soc.* **2000**, *122*, 12340–12345.
17. Tsutsui, M.; Hongo, S.; He, Y.; Taniguchi, M.; Gemma, N.; Kawai, T. Single-Nanoparticle Detection Using a Low-Aspect-Ratio Pore. *ACS Nano* **2012**, *6*, 3499–3505.
18. Wang, J.; Ma, J.; Ni, Z.; Zhang, L.; Hu, G. Effects of Access Resistance on the Resistive-Pulse Caused by Translocating of a Nanoparticle Through a Nanopore. *RSC Adv.* **2014**, *4*, 7601–7610.
19. Wanunu, M.; Dadosh, T.; Ray, V.; Jin, J.; McReynolds, L.; Drndic, M. Rapid Electronic Detection of Probe-Specific MicroRNAs Using Thin Nanopore Sensors. *Nat. Nanotechnol.* **2010**, *5*, 807–814.
20. Heins, E. A.; Siwy, Z. S.; Baker, L. A.; Martin, C. R. Detecting Single Porphyrin Molecules in a Conically Shaped Synthetic Nanopore. *Nano Lett.* **2005**, *5*, 1824–1829.
21. Vogel, R.; Willmott, G.; Kozak, D.; Roberts, G. S.; Anderson, W.; Groenewegen, L.; Glossop, B.; Barnett, A.; Turner, A.; Trau, M. Quantitative Sizing of Nano/Microparticles With a

Tunable Elastomeric Pore Sensor. *Anal. Chem.* **2011**, *83*, 3499–3506.

22. Willmott, G. R.; Vogel, R.; Yu, S. S. C.; Groenewegen, L. G.; Roberts, G. S.; Kozak, D.; Anderson, W.; Trau, M. Use of Tunable Nanopore Blockade Rates to Investigate Colloidal Dispersions. *J.Phys.: Condens. Matter* **2010**, 22.

23. Stober, G.; Steinbock, L. J.; Keyser, U. F. Modeling of Colloidal Transport in Capillaries. *J. Appl. Phys.* **2009**, 105.

24. Venta, K.; Shemer, G.; Puster, M.; Rodriguez-Manzo, J. A.; Balan, A.; Rosenstein, J. K.; Shepard, K.; Drndic, M. Differentiation of Short, Single-Stranded DNA Homopolymers in Solid-State Nanopores. *ACS Nano* **2013**, *7*, 4629–4636.

25. van den Hout, M.; Krudde, V.; Janssen, X. J. A.; Dekker, N. H. Distinguishable Populations Report on the Interactions of Single DNA Molecules With Solid-State Nanopores. *Biophys. J.* **2010**, *99*, 3840–3848.

26. Wanunu, M.; Sutin, J.; McNally, B.; Chow, A.; Meller, A. DNA Translocation Governed by Interactions With Solid-State Nanopores. *Biophys. J.* **2008**, *95*, 4716–4725.

27. Kowalczyk, S. W.; Dekker, C. Measurement of the Docking Time of a DNA Molecule onto a Solid-State Nanopore. *Nano Lett.* **2012**, *12*, 4159–4163.

28. Rosenstein, J. K.; Wanunu, M.; Merchant, C. A.; Drndic, M.; Shepard, K. L. Integrated Nanopore Sensing Platform With Sub-Microsecond Temporal Resolution. *Nat. Meth.* **2012**, *9*, 487–U112.

29. Vlassarev, D. M.; Golovchenko, J. A. Trapping DNA Near a Solid-State Nanopore. *Biophys. J.* **2012**, *103*, 352–356.

30. Smeets, R. M. M.; Keyser, U. F.; Krapf, D.; Wu, M. Y.; Dekker, N. H.; Dekker, C. Salt Dependence of Ion Transport and DNA Translocation Through Solid-State Nanopores. *Nano Lett.* **2006**, *6*, 89–95.

31. Stein, D.; Kruithof, M.; Dekker, C. Surface-Charge-Governed Ion Transport in Nanofluidic Channels. *Phys. Rev. Lett.* **2004**, 93.

32. Kowalczyk, S. W.; Dekker, C. Salt and Voltage Dependence of the Conductance Blockade Induced by Translocation of DNA and RecA Filaments Through Solid-State Nanopores. In *Nanopores for Bioanalytical Applications*; Edel, J., Albrecht, T., Eds.; Royal Society of Chemistry: London, 2012.

33. Yang, J.; Ferranti, D. C.; Stern, L. A.; Sanford, C. A.; Huang, J.; Ren, Z.; Qin, L.-C.; Hall, A. R. Rapid and Precise Scanning Helium Ion Microscope Milling of Solid-State Nanopores for Biomolecule Detection. *Nanotechnology* **2011**, *22*, 285310.

34. Aksimentiev, A.; Heng, J. B.; Timp, G.; Schulten, K. Microscopic Kinetics of DNA Translocation Through Synthetic Nanopores. *Biophys. J.* **2004**, *87*, 2086–2097.

35. Lu, B.; Albertorio, F.; Hoogerheide, D. P.; Golovchenko, J. A. Origins and Consequences of Velocity Fluctuations During DNA Passage Through a Nanopore. *Biophys. J.* **2011**, *101*, 70–79.

36. Storm, A. J.; Storm, C.; Chen, J. H.; Zandbergen, H.; Joanny, J. F.; Dekker, C. Fast DNA Translocation through a Solid-State Nanopore. *Nano Lett.* **2005**, *5*, 1193–1197.

37. Chen, P.; Gu, J. J.; Brandin, E.; Kim, Y. R.; Wang, Q.; Branton, D. Probing Single DNA Molecule Transport Using Fabricated Nanopores. *Nano Lett.* **2004**, *4*, 2293–2298.

38. Mandel, M. The Electrical Polarization of Rod-Like Charged Macromolecules. *Mol. Phys.* **1961**, *4*, 489–469.

39. Manning, G. S. A Condensed Counterion Theory for Polarization of Polyelectrolyte Solutions in High Fields. *J. Chem. Phys.* **1993**, *99*, 477–486.

40. Mohanty, U.; Zhao, Y. Q. Polarization of Counterions in Polyelectrolytes. *Biopolymers* **1996**, *38*, 377–388.

41. Rau, D. C.; Charney, E. Polarization of the Ion Atmosphere of a Charged Cylinder. *Biophys. Chem.* **1981**, *14*, 1–9.

42. Elvingson, C. Computer Simlations of the Structure of DNA Molecules in an Electric Field. *Biophys. Chem.* **1992**, *43*, 9–19.

43. Netz, R. R. Polyelectrolytes in Electric Fields. *J. Phys. Chem. B* **2003**, *107*, 8208–8217.

44. Yoshida, M.; Kikuchi, K.; Maekawa, T.; Watanabe, H. Electric Polarization of Rodlike Polyions Investigated by Monte-Carlo Simulations. *J. Phys. Chem.* **1992**, *96*, 2365–2371.

45. Diekmann, S.; Hillen, W.; Jung, M.; Wells, R. D.; Porschke, D. Electric Properties and Structure of DNA Restriction Fragments From Measurements of the Electrical Dichroism. *Biophys. Chem.* **1982**, *15*, 157–167.

46. Diekmann, S.; Jung, M.; Teubner, M. On the Orientation Function of the Electric Dichroism of DNA. *J. Chem. Phys.* **1984**, *80*, 1259–1262.

47. Porschke, D. The Mechanism of Ion Polarization Along DNA Double Helices. *Biophys. Chem.* **1985**, *22*, 237–247.

48. Chang, H.; Venkatesan, B. M.; Iqbal, S. M.; Andreadakis, G.; Kosari, F.; Vasmatzis, G.; Peroulis, D.; Bashir, R. DNA Counterion Current and Saturation Examined by a MEMS-Based Solid State Nanopore Sensor. *Biomed. Microdevices* **2006**, *8*, 263–269.

49. Das, S.; Dubsky, P.; van den Berg, A.; Eijkel, J. C. T. Concentration Polarization in Translocation of DNA Through Nanopores and Nanochannels. *Phys. Rev. Lett.* **2012**, 108.

50. Comer, J.; Dimitrov, V.; Zhao, Q.; Timp, G.; Aksimentiev, A. Microscopic Mechanics of Hairpin DNA Translocation Through Synthetic Nanopores. *Biophys. J.* **2009**, *96*, 593–608.

51. Luan, B.; Aksimentiev, A. Electro-Osmotic Screening of the DNA Charge in a Nanopore. *Phys. Rev. E* **2008**, 78.

52. Yoo, J.; Aksimentiev, A. Competitive Binding of Cations to Duplex DNA Revealed Through Molecular Dynamics Simulations. *J. Phys. Chem. B* **2012**, *116*, 12946–12954.

53. Singer, A.; Rapireddy, S.; Ly, D. H.; Meller, A. Electronic Barcoding of a Viral Gene at the Single-Molecule Level. *Nano Lett.* **2012**, *12*, 1722–1728.

54. Garaj, S.; Hubbard, W.; Reina, A.; Kong, J.; Branton, D.; Golovchenko, J. A. Graphene as a Subnanometre Trans-Electrode Membrane. *Nature* **2010**, *467*, 190–U73.

55. Garaj, S.; Liu, S.; Golovchenko, J. A.; Branton, D. Molecule-Hugging Graphene Nanopores. *Proc. Natl. Acad. Sci. U.S.A.* **2013**, *110*, 12192–12196.

56. Merchant, C. A.; Healy, K.; Wanunu, M.; Ray, V.; Peterman, N.; Bartel, J.; Fischbein, M. D.; Venta, K.; Luo, Z. T.; Johnson, A. T. C.; et al. DNA Translocation Through Graphene Nanopores. *Nano Lett.* **2010**, *10*, 2915–2921.

57. Schneider, G. F.; Kowalczyk, S. W.; Calado, V. E.; Pandraud, G.; Zandbergen, H. W.; Vandersypen, L. M. K.; Dekker, C. DNA Translocation Through Graphene Nanopores. *Nano Lett.* **2010**, *10*, 3163–3167.

58. Traversi, F.; Raillon, C.; Benameur, S. M.; Liu, K.; Khlybov, S.; Tosun, M.; Krasnozhon, D.; Kris, A.; Radenovic, A. Detecting the Translocation of DNA Through a Nanopore Using Graphene Nanoribbons. *Nat. Nanotechnol.* **2013**, *8*, 939–945.

59. Marshall, M. M.; Yang, J.; Hall, A. R. Direct and Transmission Milling of Suspended Silicon Nitride Membranes With a Focused Helium Ion Beam. *Scanning* **2012**, *34*, 101–106.

60. Hall, A. R. *In Situ* Thickness Assessment During Ion Milling of a Free-Standing Membrane Using Transmission Helium Ion Microscopy. *Microsc. Microanal.* **2013**, *19*, 740–744.